Capillarity
Vol. 17, No. 2, p. 68-76, 2025

Original article

Spontaneous imbibition of quasi-linear viscoelastic fluids

Shengda Sun[1], Guodong Wang[1], Senlin Zhu[1], Ruoyu Dong[1,2], Qingfei Fu[1,3], Chiyu Xie[1,2,3]*

[1]School of Astronautics, Beihang University, Beijing 102206, P. R. China
[2]State Key Laboratory of High-Efficiency Reusable Aerospace Transportation Technology, Beijing 102206, P. R. China
[3]Ningbo Institute of Technology, Beihang University, Ningbo 315100, P. R. China

Keywords:
Spontaneous imbibition
Oldroyd-B fluid
viscoelastic fluid
capillary flow
interfacial tension

Cited as:
Sun, S., Wang, G., Zhu, S., Dong, R., Fu, Q., Xie, C. Spontaneous imbibition of quasi-linear viscoelastic fluids. Capillarity, 2025, 17(2): 68-76.
https://doi.org/10.46690/capi.2025.11.03

Abstract:
Spontaneous imbibition phenomena are commonly observed in capillaries and porous media. The extraction of energy resources, lubrication in the machinery industry, and therapeutic applications in life sciences often involve the imbibition of complex viscoelastic non-Newtonian fluids. Although the imbibition of Newtonian fluids or simple linear Maxwell viscoelastic fluids have been well studied, investigations on the imbibition of quasi-linear or nonlinear viscoelastic fluids are still rare. This paper focuses on the imbibition mechanism of quasilinear viscoelastic fluids. Primarily, the theoretical relationship between the imbibition height and time for quasi-linear fluid in a single capillary tube is derived, by incorporating the elastic stress into the classical Lucas-Washburn imbibition theory for Newtonian fluids. Then, glass capillary imbibition experiments are performed to validate the theoretical predictions, showing good agreements. Moreover, the impacts of key viscoelastic features on the imbibition of fluids are investigated, including the viscosity ratio and the relaxation time. The results show that under the capillary dominated conditions, the imbibition rate increases with the viscosity ratio, and this trend is more pronounced at larger relaxation time. In addition, the study finds a critical Deborah number , under which the viscoelastic effect is negligible. Conversely, when the viscoelasticity is strong, the imbibition height and velocity of fluids decrease with increasing relaxation time in a nonlinear manner. The study provides important theoretical support and guidance for engineering problems involving capillary action of viscoelastic fluids, advancing the understanding of the imbibition mechanisms of non-Newtonian fluids.

1. Introduction

Spontaneous imbibition refers to the phenomenon that the wetting fluid can infiltrate a porous medium due to the capillary forces spontaneously at the liquid-gas-solid interface (Washburn, 1921). It plays a vital role in various natural and industrial processes (Tani et al., 2015; Wang et al., 2022), such as energy resource extraction (Roychaudhuri et al., 2013; Cai et al., 2020; Xia et al., 2023), lubrication in mechanical systems (Chen et al., 2022; Zhang et al., 2023; Leyva et al., 2024), and applications in the life sciences (Jung et al., 2020; Farzan et al., 2023). In energy resource extraction, imbibition enhances oil and shale gas recovery by driving water or surfactant solutions into rock pores, thereby improving recovery efficiency (Mason and Morrow, 2013; Sheng, 2017; Zheng et al., 2021; Cai et al., 2023). In mechanical systems, optimizing the pore structure of materials enables effective storage, release, and recovery of lubricants, thus enhancing lubrication performance and prolonging the service life of equipment (Zhang et al., 2023; Chakraborty, 2025). In life sciences, imbibition is widely used in drug delivery, tissue

Yandy Scientific Press

*Corresponding author.
E-mail address: sunshengda@buaa.edu.cn (S. Sun); w2585863028@gmail.com (G. Wang); slzhu@buaa.edu.cn (S. Zhu); dongry@buaa.edu.cn (R. Dong); fuqingfei@buaa.edu.cn (Q. Fu); xiechiyu@buaa.edu.cn (C. Xie).

Received September 4, 2025; revised September 29, 2025; accepted October 17, 2025; available online October 20, 2025.

engineering, and biomaterials. In plants, it is essential for water and nutrient uptake and transport (Farzan et al., 2023).

The fluids in the above processes are often complex non-Newtonian viscoelastic fluids that exhibit both solid and liquid properties (Sonker et al., 2021; Xie et al., 2022a, 2022b; Benavent-Claró et al., 2024). Therefore, understanding the spontaneous imbibition of viscoelastic fluids is critical for advancing energy recovery, improving lubrication performance, and achieving precise biomedical treatments, etc.

The imbibition of Newtonian fluids has been extensively studied, including a serious of advancements in theoretical frameworks (Vachaparambil and Einarsrud, 2019; Cai et al., 2021; Cai et al., 2022). Washburn (1921) seminal work introduced the Lucas-Washburn (LW) equation and the concept of permeability, laying the foundation for understanding fluid flow in porous media. Bosanquet (1923) extended it by examining the kinetic behavior of fluids entering capillaries, particularly the influence of fluid momentum, and developed equations for motion and dynamic surface tension measurement. Fries and Dreyer (2009) applied the π-theorem to derive a dimensionless scaling approach and analyzed dynamics under various scaling strategies. Gründing et al. (2020) compared the capillary rise between parallel plates obtained by numerical methods such as Arbitrary Lagrangian-Eulerian, Volume of Fluid and level-set techniques to an ordinary differential equation model, with special emphasis on the slip length effects. Yang and Wang (2023) used the multiphase lattice Boltzmann method to conduct a three-dimensional simulation of the influence of dynamic wettability during the imbibition process. Yang et al. (2025) established a fractal model for fluid imbibition in irregular rough pores and derived the expressions for imbibition height and imbibition amount in irregular rough pores.

Studies on the imbibition of non-Newtonian fluids starts from simple rheological models (Gosselin et al., 2016; Gorthi et al., 2020; Asadi et al., 2023). Shan et al. (2020) generalized the LW equation to model the dynamics of power-law fluids in capillaries, incorporating nonlinearity, power-law exponents, and displaced fluid effects. Asadi et al. (2023) developed a generalized Richards equation to predict spontaneous absorption behavior in high-shear dilute fluids relevant to gas exploration. Gosselin et al. (2016) experimentally examined the rheological and filling behavior of whole blood in capillaries. Kornev and Neimark (2003) theoretically studied the spontaneous imbibition of viscoelastic fluids using the Maxwell model, highlighting the role of elasticity and the Weissenberg number. Bandopadhyay and Chakraborty (2014) used a Phan-Thien-Tanner model to investigate viscoelastic fluid filling in both horizontal and vertical capillaries, analyzing the influence of gravity and rheology on oscillatory behavior. Thompson and Oishi (2021) explored the roles of Reynolds and Weissenberg numbers in viscoelastic flow and emphasized the Oldroyd-B model's significance for benchmarking viscoelastic behavior (Hayat et al., 2004; Brandi et al., 2019; Khalid et al., 2021; Xie et al., 2021).

While extensive researchers have addressed the linear viscoelastic fluid imbibition, there remains a lack of systematic study on the imbibition of quasi-linear or nonlinear viscoelastic fluids. Therefore, this study focuses on theoretical and experimentally investigating the imbibition behavior of quasilinear Oldroyd-B viscoelastic fluids. The elastic stress components of the Oldroyd-B model are integrated into the classical LW framework to derive a time-dependent imbibition height equation for single capillaries. Glass capillary experiments are conducted, and the effects of relaxation time and viscosity ratio are analyzed under capillary-dominated conditions (Capillary number, $\mathrm{Ca} < 10^{-2}$), (Gründing et al., 2020). The rest of this paper is organized as follows: Section 2 presents the mathematical model and experimental methods; Section 3 discusses results and evaluates the study's strengths and limitations; Section 4 concludes the work.

2. Methodology

2.1 Mathematical model

The schematic of the imbibition problem is shown in Fig. 1, where the Fluids 1 (in orange) climb into the capillary from the bottom pool due to capillary force. The background Fluid 2 is air (whose resistance is neglected), the contact angle is α (Hamraoui et al., 2000), and the interfacial tension is γ. Both fluids are considered incompressible. The study first reviews the classic LW theory (Washburn, 1921) for Newtonian fluid imbibition. Then the elastic stress is introduced to derive the spontaneous imbibition model for the Oldroyd-B fluid.

2.1.1 The LW model for Newtonian fluids

First, a physical model needs to be established. Fig. 1(a) shows the force analysis of Newtonian fluid imbibition, where the LW model can be applied to describe the change of imbibition height with time. The LW model considers quasi-static processes, and the velocity profile of Fluid 1 follows the Poiseuille's law. Therefore, the study has Eq. (1)-the relationship between rising velocity and driving pressure as (Washburn, 1921):

$$\frac{\mathrm{d}L}{\mathrm{d}t} = \frac{R^2 P_c}{8\eta L} \tag{1}$$

where t is time; R is capillary radius; P_c is the capillary pressure; η is dynamic viscosity; L is imbibition height.

The capillary pressure P_c is determined by the Young-Laplace law as:

$$P_c = \frac{2\gamma\cos\alpha}{R} \tag{2}$$

By substituting Eq. (2) into Eq. (1) and integrating it, the relationship between height and time in LW equation can be obtained as:

$$L(t) = \sqrt{\frac{\gamma R\cos\alpha}{2\eta}t} \tag{3}$$

where the imbibition height is proportional to the root time. Despite its simplified assumptions, the LW model remains a cornerstone for understanding capillary-driven flows and serves as the basis for the extension to non-Newtonian fluids.

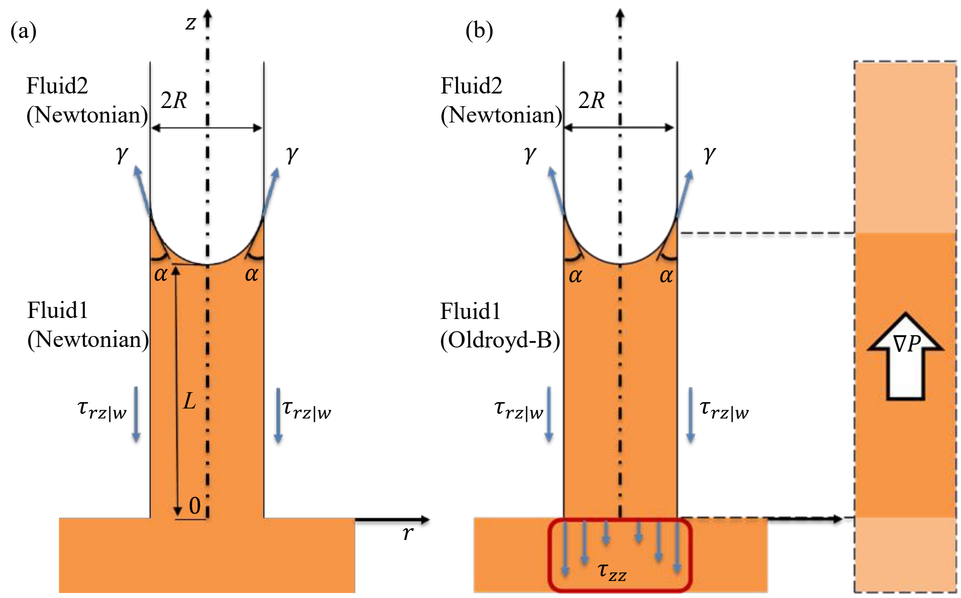

Fig. 1. Schematic diagram of the imbibition of (a) a Newtonian fluid and (b) an Oldroyd-B fluid.

2.1.2 The Oldroyd-B fluid imbibition model

Next, elastic force needs to be introduced. Fig. 1(b) shows the force analysis of the Oldroyd-B fluid imbibition model. The main difference between the Oldroyd-B fluid and Newtonian fluid is that the Oldroyd-B fluid bears not only shear force but also elastic force. The fluid bear shear stress $\tau_{rz|w}$ at the wall surface of the tube and the tensile stress τ_{zz} at the bottom of the tube. The total viscous force F_v and the elastic force F_e are balanced with the capillary force F_c (Bandopadhyay and Chakraborty, 2014; Li and Fontelos, 2023) as:

$$F_c = F_v + F_e \tag{4}$$

where

$$F_c = 2\pi R\gamma \cos\alpha \tag{5}$$

$$F_v = 2\pi R z \tau_{rz|w}(r = R) \tag{6}$$

$$F_e = \int_0^R 2\pi r \tau_{zz} \mathrm{d}r \tag{7}$$

Next, the Eqs. (6) and (7) are to obtain the stress expressions including the wall shear force $\tau_{rz|w}$ and bottom elastic stress τ_{zz}.

The constitutive equation of Oldroyd-B viscoelastic fluid is given by Oldroyd (1950) as:

$$\boldsymbol{\tau} + \lambda_1 \overset{\nabla}{\boldsymbol{\tau}} = 2\eta_0 \left(\boldsymbol{D} + \lambda_2 \overset{\nabla}{\boldsymbol{D}}\right) \tag{8}$$

where $\boldsymbol{\tau}$ is the stress tensor; λ_1 is the relaxation time; $\lambda_2 = \lambda_1 \eta_s/\eta_0$ is the retardation time; $\beta = \eta_s/\eta_0$ is viscosity ratio; $\eta_0 = \eta_s + \eta_p$ is the total viscosity consisting of the solvent and the polymer components; $\overset{\nabla}{\boldsymbol{\tau}} = \partial\boldsymbol{\tau}/\partial t + \boldsymbol{U}\cdot\nabla\boldsymbol{\tau} - (\nabla\boldsymbol{U})^T\cdot\boldsymbol{\tau} - \boldsymbol{\tau}\cdot(\nabla\boldsymbol{U})$ is the upper convective time derivative of the stress tensor; $\boldsymbol{D} = [\nabla\boldsymbol{U} + (\nabla\boldsymbol{U})^T]/2$ is the deformation rate tensor or strain rate tensor, $\boldsymbol{U}$ is velocity vector.

Following Morozov and van Saarloos (2019) and Boyko and Stone (2022), for pressure-driven flow in a capillary, the velocity profile is:

$$u_z(r) = \frac{\nabla P}{4\eta_0}(R^2 - r^2) \tag{9}$$

where ∇P is pressure gradient; $u_z(r)$ is axial velocity; r is radial distance.

The stress components are:

$$\tau_{rz} = \eta_0 \left[\frac{\partial u_z(r)}{\partial r}\right] = \frac{\nabla P r}{2} \tag{10}$$

$$\tau_{zz} = 2\eta_p\lambda_1 \left[\frac{\partial u_z(r)}{\partial r}\right]^2 = \frac{\eta_p\lambda_1(\nabla P)^2 r^2}{2\eta_0^2} \tag{11}$$

Substituting the stress Eqs. (10) and (11) into Eqs. (6) and (7) can get:

$$F_v = \pi R^2 \nabla P z \tag{12}$$

$$F_e = \frac{\pi\eta_p\lambda_1(\nabla P)^2 R^4}{4\eta_0^2} \tag{13}$$

Combing Eqs. (4), (12) and (13), ∇P as a function of imbibition height z can be obtained as:

$$\nabla P = f(z) = \frac{\sqrt{(Rz)^2 + \dfrac{2\eta_p\lambda_1 R^3\gamma\cos\alpha}{\eta_0^2}} - Rz}{\dfrac{\eta_p\lambda_1 R^3}{2\eta_0^2}} \tag{14}$$

where ∇P is composed of capillary force, viscous force, and elastic force.

According to Eq. (9), the interface velocity at the mean interface height L can be expressed as:

$$\frac{\mathrm{d}L}{\mathrm{d}t} = \frac{\nabla P R^2}{8\eta_0} \tag{15}$$

Finally, by substituting Eq. (14) into Eq. (15), the imbibition speed of the quasi-linear viscoelastic Oldroyd-B fluid can be obtained as:

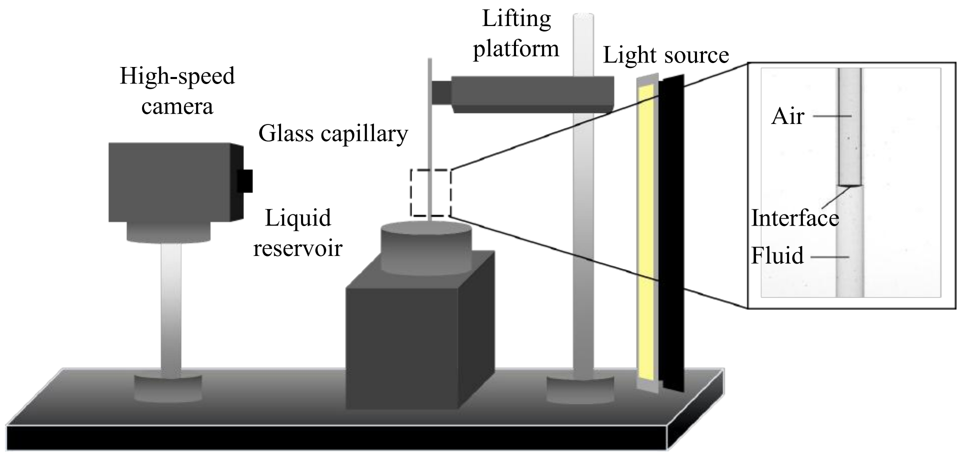

Fig. 2. Schematic diagram of the experimental platform.

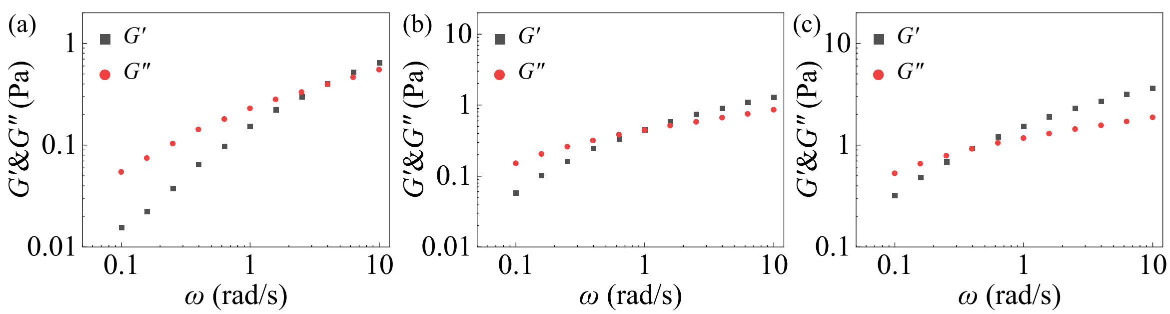

Fig. 3. Modulus of storage vs. loss modulus curves: (a) $F1$, (b) $F2$ and (c) $F3$.

$$\frac{\mathrm{d}L}{\mathrm{d}t}=\frac{\eta_0}{4\eta_p\lambda_1 R}\left[\sqrt{(RL)^2+\frac{2\eta_p\lambda_1 R^3\gamma\cos\alpha}{\eta_0^2}}-RL\right] \tag{16}$$

And the imbibition height L can be implicitly obtained by integrating Eq. (16) over time.

The effect of elastic force is reflected in λ_1 and η_p, which is the main difference from Newtonian fluid imbibition.

2.2 Experiment configuration

The study also performs experiments to verify the theoretical expressions. Fig. 2 is a schematic diagram of the experimental platform, which mainly includes five parts: High-speed camera, glass capillary, liquid reservoir, lifting platform and light source. The capillary tube (with length of 10 cm, diameter of 300 μm and surface roughness below 5%) is vertically fixed to a lift platform and brought into contact with the viscoelastic fluid reservoir. The liquid rise and gas-liquid interface dynamics are recorded by a high-speed camera, allowing clear visualization of the imbibition process. The reservoir's size is significantly larger than the capillary's characteristic length, thereby minimizing boundary effects and ensuring uniform wetting conditions.

The experimental conditions fall into the capillary forces dominated condition with negligible inertial effects, where the capillary number $\mathrm{Ca} < 10^{-2}$ and the Reynolds number $\mathrm{Re} < 0.1$ (Li et al., 2023).

The viscoelastic fluids in this work are prepared using polyethylene oxide (PEO, molecular weight: 8×10^6 g/mol) and polyethylene glycol (PEG, molecular weight: 6,000 g/mol) dissolved in deionized water, which served as the solvent. The solvent's viscosity is 1 mPa·s. The rheological properties of the solutions are measured using an Anton Paar MCR 302 rheometer. Fig. 3 shows the oscillation curves of the storage modulus (G') and loss modulus (G''). Viscoelastic properties are characterized by oscillation patterns, and the relaxation time of each Oldroyd-B fluid is determined based on the inverse frequency of the crossover point between G' and G'' (Kraft et al., 1999; Niedzwiedz et al., 2008). The relaxation times of the three tested solutions are 0.25, 1, and 2.5 s, respectively, indicating a gradual increase in viscoelastic properties. The specific compositions and corresponding rheological parameters are listed in Table 1.

3. Results and discussion

3.1 Experimental validation of the Oldroyd-B imbibition model

Comparative experiments are conducted on different viscoelastic fluids. Figs. 4(a)-4(c) illustrates the imbibition behavior of fluids $F1$, $F2$ and $F3$, respectively. It is observed that the imbibition height increases with time, while the rate of rise gradually decreases. In the initial stage of imbibition, the capillary force is the dominant driving factor, and resistive forces such as viscous and elastic stresses are relatively small,

Table 1. Fluid properties.

Fluid	Molecular weight (g/mol)	Total mass fraction wt.% (-)	Viscosity@20 °C (mPa·s)	Relaxation time (s)	Contact Angle (°)	Interfacial tension (N/m)
$F1$	8×10^6 PEO 6,000 PEG	0.3% PEO 1% PEG	32	0.25	20	0.043
$F2$	8×10^6 PEO 6,000 PEG	0.4% PEO 1% PEG	50	1	20	0.045
$F3$	8×10^6 PEO 6,000 PEG	0.6% PEO 1% PEG	96	2.5	20	0.045

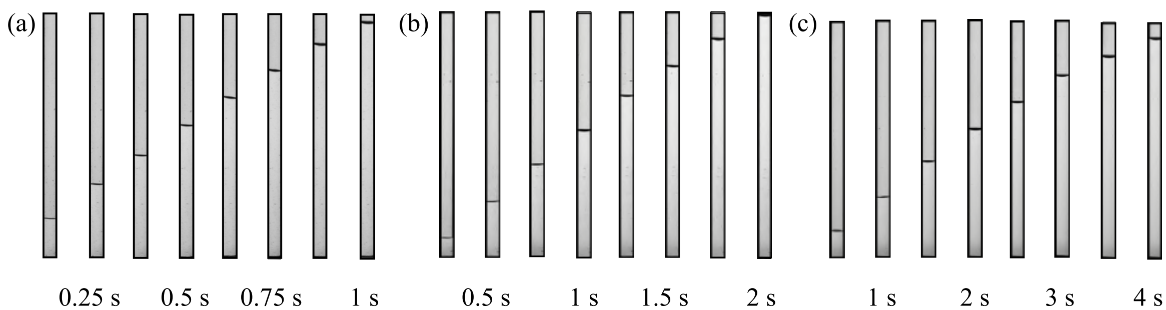

Fig. 4. Imbibition processes obserbed in experiments of Fluids (a) $F1$, (b) $F2$ and (c) $F3$.

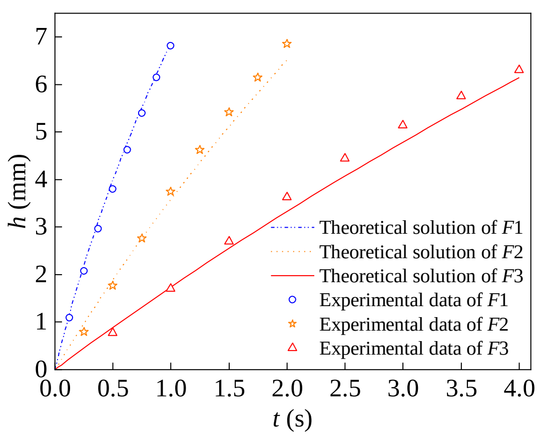

Fig. 5. Comparisons of experimental results with theoretical solutions.

resulting in a rapid imbibition rate. As the imbibition height increases, both viscous and elastic resistances grow, leading to a progressive slowdown in the imbibition rate. Additionally, fluids with longer relaxation times exhibit stronger viscoelastic behavior, which further reduces the imbibition speed. Fig. 5 compares the experimental results with theoretical predictions. The model shows good agreement with experimental data, with an average error of less than 5%, thereby confirming the accuracy of the theoretical expressions.

3.2 The effect of viscosity ratio

The study further examined the influence of viscosity ratio and relaxation time on the imbibition rate of Oldroyd-B viscoelastic fluids. The results, presented as the variation of imbibition height over time for different viscosity ratios β, reveal key trends. Here, the total viscosity of the Oldroyd-B fluid is $\eta_0 = 0.1$ Pa·s, the wetting angle is $\alpha = 45°$, the interfacial tension is $\gamma = 0.02$ N/m, and the capillary tube diameter is $d = 200$ µm. Figs. 6(a) and 6(b) correspond to imbibition result at relaxation times of 0.1 s and 1 s. It is observed that the imbibition rate increases with an increase in viscosity ratio throughout the process. However, this trend becomes more pronounced only at higher relaxation times. When the relaxation time is small, the effect of the viscosity ratio on the imbibition rate is minimal. This is because, at low viscoelasticity, the fluid behavior approaches that of a Newtonian fluid. As the relaxation time increases, the influence of the viscoelastic stress described by the Oldroyd-B model becomes more significant, thereby accelerating the imbibition rate.

3.3 The effect of relaxation time

In addition, the impact of viscoelasticity on the imbibition process is discussed by changing the relaxation time. First, the numerical computation set that the viscosity is $\eta_0 = 0.1$ Pa·s, the viscosity ratio is $\beta = 0.1$, the wetting angle is $\alpha = 45°$, and the interfacial tension is $\gamma = 0.02$ N/m. The relaxation times considered are 0.001, 0.005, 0.01, 0.05, 0.1, 0.5, 1, and 5 s, and a capillary tube diameter of $d = 200$ µm. Fig. 7(a) presents the variation of imbibition height with time for different relaxation times. It is evident that the imbibition height decreases with increasing relaxation time at each time point. Fig. 7(b) shows the variation of imbibition velocity over time. The imbibition process lasts for 5 s, during which the velocity gradually

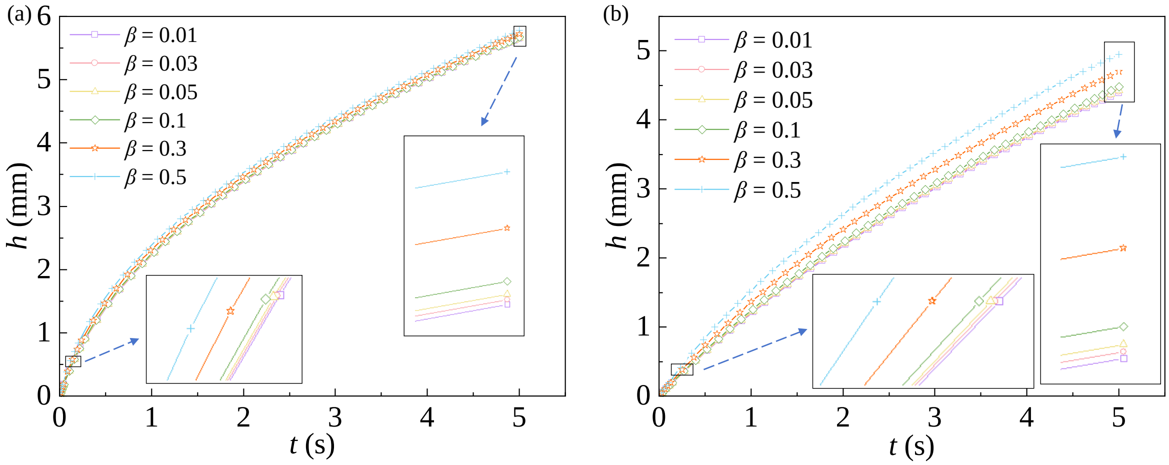

Fig. 6. Imbibition at different viscosity ratios: (a) $\lambda = 0.1$ s and (b) $\lambda = 1$ s (The error caused by the time step from 1,000 to 100,000 is less than 1%).

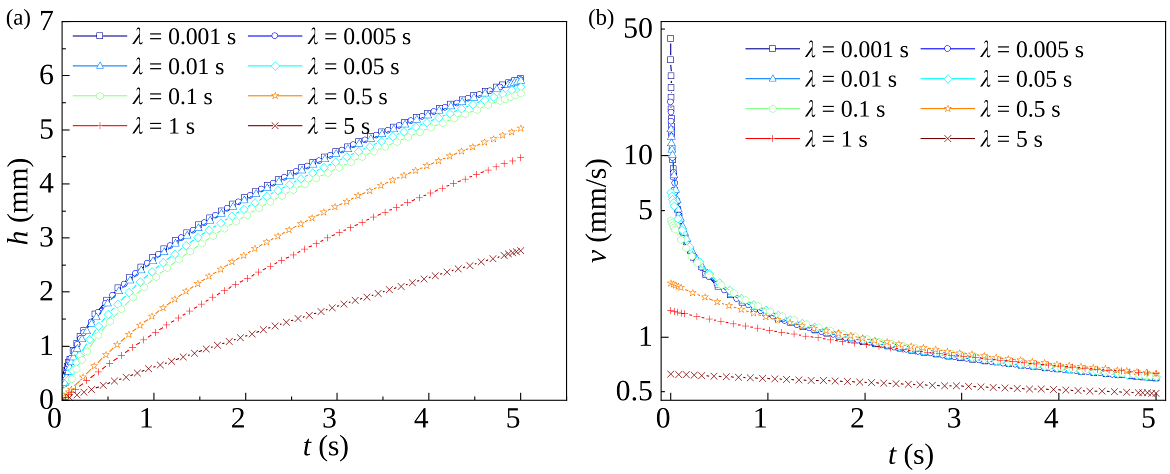

Fig. 7. Imbibition at different relaxation times: (a) Imbibition height and (b) imbibition rate (The error caused by the time step from 1,000 to 100,000 is less than 1%).

stabilizes. For relaxation times between 0.001s and 0.1 s, the differences in imbibition height are relatively minor. However, when the relaxation time ranges from 0.5 to 5 s, the imbibition height exhibits a significant dependence on the relaxation time, indicating a stronger influence of fluid elasticity at longer relaxation times.

To quantitatively calculate the effect of relaxation time on the imbibition height under the dominance of capillary force ($\text{Ca} < 10^{-2}$), the different diameters ($d = 100, 300, 500$ and 600 μm) were set with other parameters remain unchanged. Fig. 8(a) illustrates the relationship between relaxation time and the imbibition height at 5 s for capillaries with different diameters. The results indicate that the imbibition height decreases as the relaxation time increases. Additionally, larger capillary diameters facilitate faster imbibition. Compared with the case of zero relaxation time, the imbibition height decreases by approximately 4.5% at a relaxation time of 0.1 s, and by 15.5% at 0.5 s. These observations underscore the critical role of relaxation time in the imbibition process, as it directly influences the development of elastic stress, which significantly affects the fluid's imbibition capacity. Once the elastic stress reaches a certain threshold, its influence can no longer be neglected.

Next, dimensionless analysis is performed. Fig. 8(b) further presents the relationship between the Deborah number ($\text{De} = u_z \lambda_1 / 2R$) and the normalized imbibition height. When the De is small, the imbibition height remains relatively constant despite increasing relaxation time. However, at higher De numbers, the imbibition height decreases markedly with increasing relaxation time. This behavior can be attributed to the enhanced elastic forces associated with larger relaxation times, which increase flow resistance and thereby reduce the imbibition height. There is a competitive relationship between elastic stress and capillary driving force. Capillary force is the driving force in the imbibition movement, while elastic stress plays a hindering role. When the De number reaches a certain range, the influence of elastic force will be very large. Specifically, when $\text{De} > 0.85$, the imbibition height decreases by approximately 10% compared to the case with $\text{De} = 0$. These findings indicate that the elastic stress characteristic of Oldroyd-B viscoelastic fluids must be fully accounted for when De exceeds this threshold.

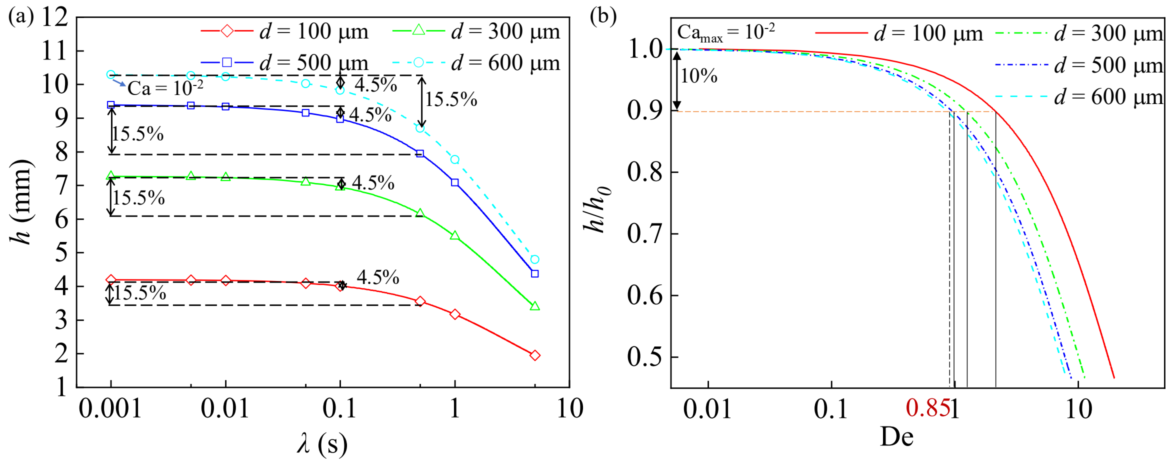

Fig. 8. Imbibition in capillaries with different sizes: (a) Relaxation time vs. imbibition height and (b) De number vs. normalized height.

In this study, the imbibition of Oldroyd-B viscoelastic fluids is systematically investigated. By incorporating the elastic force characteristic of Oldroyd-B fluids into the classical LW model and accounting for the kinetic factors influencing viscoelastic fluid imbibition, a theoretical framework describing the evolution of imbibition height in a single capillary tube is developed. The theoretical model is validated through glass capillary experiments, confirming its accuracy and applicability.

For the effect of viscosity ratio, the imbibition rate increased with increasing viscosity ratio, and this trend became more pronounced with increasing relaxation time, reflecting enhanced viscoelastic behavior, which highlights the critical role of elastic stresses in modulating flow resistance during imbibition. For the elastic effects: When the relaxation time is small, its effect on imbibition height is minimal; however, as the relaxation time increased, the imbibition height decreased significantly, primarily due to the growing contribution of elastic stress, which opposes capillary-driven motion. A dimensionless analysis revealed that when the De > 0.85, the imbibition rate exhibits a marked decline. This behavior confirms that increased relaxation time leads to higher elastic stress, which increasingly counteracts the capillary force and impairs imbibition performance.

While this work offers valuable insights into the complex imbibition behavior of nonlinear viscoelastic fluids and identifies key influencing parameters, certain limitations remain. Specifically, the relative contributions of various forces during different imbibition stages are not quantitatively assessed, and the number of experimental cases analyzed is limited, potentially affecting the generalizability of the conclusions. Future work will extend the study to more complex geometries (e.g., curved capillaries, porous networks), as well as compare with other nonlinear viscoelastic models (e.g., Giesekus, Phan-Thien-Tanner).

4. Conclusions

In this work, a modified theoretical model that describes the height-time relationship for Oldroyd-B fluids imbibition in a single capillary tube is presented by incorporating the elastic stress into the classical LW theory. Glass capillary imbibition experiments are conducted, and the measured height-time curves show close agreement with the theoretical predictions, confirming the validity of the model. Under capillarity-dominated conditions (Ca $< 10^{-2}$), systematic analysis reveals that the imbibition rate increases with the viscosity ratio, with the enhancement becoming more pronounced at larger relaxation times. A critical De number of approximately 0.85 is identified: For De < 0.85, viscoelastic effects are negligible and relaxation time exerts minimal influence on the imbibition process; for De > 0.85, strong viscoelasticity leads to a nonlinear reduction in imbibition height and velocity with increasing relaxation time, for which elastic stress plays a non-ignorable role. These findings advance the mechanistic understanding of capillary imbibition in quasi-linear viscoelastic fluids and provide a theoretical basis for engineering applications involving capillarity-driven flows of non-Newtonian fluids.

Acknowledgements

This work is supported by the National Natural Science Foundation of China (Nos. 12302326 and U2341281) and the PetroChina Technical Program (No. 2023DJ84). Mr. Sun thanks Mr. Zihao Dong for the help on experimental discussions.

Conflict of interest

The authors declare no competing interest.

References

Asadi, H., Pourjafar-Chelikdani, M., Taghavi, S. M., et al. Development of a generalized Richards equation for predicting spontaneous imbibition of highly shear-thinning liquids in gas recovery applications. Physics of Fluids, 2023, 35(3): 033104.

Bandopadhyay, A., Chakraborty, S. Capillary filling dynamics of viscoelastic fluids. Physical Review E, 2014, 89: 053024.

Benavent-Claró, A., Granados Leyva, S., Pagonabarraga, I., et al. Enhanced imbibition in liquid-infused coated microchannels. Langmuir, 2024, 40(50): 26600-26606.

Bosanquet, C. H. On the flow of liquids into capillary tubes. Philosophical Magazine, 1923, 45: 525-531.

Boyko, E., Stone, H. A. Pressure-driven flow of the viscoelastic Oldroyd-B fluid in narrow non-uniform geometries: Analytical results and comparison with simulations. Journal of Fluid Mechanics, 2022, 936: A23.

Brandi, A. C., Mendonça, M. T., Souza, L. F., et al. DNS and LST stability analysis of Oldroyd-B fluid in a flow between two parallel plates. Journal of Non-Newtonian Fluid Mechanics, 2019, 267: 14-27.

Cai, J., Chen, Y., Liu, Y., et al. Capillary imbibition and flow of wetting liquid in irregular capillaries: A 100-year review. Advances in Colloid and Interface Science, 2022, 304: 102654.

Cai, J., Jin, T., Kou, J., et al. Lucas-Washburn equation-based modeling of capillary-driven flow in porous systems. Langmuir, 2021, 37(5): 1623-1636.

Cai, J., Li, C., Song, K., et al. The influence of salinity and mineral components on spontaneous imbibition in tight sandstone. Fuel, 2020, 269: 117087.

Cai, J., Sun, S., Wang, H. Current advances in capillarity: Theories and applications. Capillarity, 2023, 7(2): 25-31.

Chakraborty, S. Dynamics of capillary flow of blood into a microfluidic channel. Lab on a Chip, 2025, 5(4): 421-430.

Chen, W., Wang, W., Liang, H., et al. Study on lubricant release-recycle performance of porous polyimide retainer materials. Langmuir, 2022, 38: 11440-11450.

Farzan, M., Roth, R., Schoelkopf, J., et al. The processes behind drug loading and release in porous drug delivery systems. European Journal of Pharmaceutics and Biopharmaceutics, 2023, 189: 133-151.

Fries, N., Dreyer, M. Dimensionless scaling methods for capillary rise. Journal of Colloid and Interface Science, 2009, 338: 514-518.

Gorthi, S. R., Meher, S. K., Biswas, G., et al. Capillary imbibition of non-Newtonian fluids in a microfluidic channel: Analysis and experiments. Proceedings of the Royal Society A, 2020, 476(2242): 20200496.

Gosselin, D.,Huet, M., Cubizolles, M., et al. Viscoelastic capillary flow: The case of whole blood. AIMS Biophysics, 2016, 3: 340-357.

Gründing, D., Smuda, M., Antritter, T., et al. A comparative study of transient capillary rise using direct numerical simulations. Applied Mathematical Modelling, 2020, 86: 142-165.

Hamraoui, A., Thuresson, K., Nylander, T., et al. Can a dynamic contact angle be understood in terms of a friction coefficient?. Journal of Colloid and Interface Science, 2000, 226(2): 199-204.

Hayat, T., Khan, M., Ayub, M. Exact solutions of flow problems of an Oldroyd-B fluid. Applied Mathematics and Computation, 2004, 151(1): 105-119.

Jung, S., Kim, W., Kim, H. Dynamics of liquid imbibition through partially soluble porous sheets. JMST Advances, 2020, 2: 53-59.

Khalid, M., Chaudhary, I., Garg, P., et al. The centre-mode instability of viscoelastic plane Poiseuille flow. Journal of Fluid Mechanics, 2021, 915: A43.

Kornev, K. G., Neimark, A. V. Modeling of spontaneous penetration of viscoelastic fluids and biofluids into capillaries. Journal of Colloid and Interface Science, 2003, 262: 253-262.

Kraft, M., Meissner, J., Kaschta, J. Linear viscoelastic characterization of polymer melts with long relaxation times. Macromolecules, 1999, 32(3): 751-757.

Leyva, S. G., Pagonabarraga, I., Hernández-Machado, A., et al. Capillary imbibition in lubricant-coated channels. Physical Review Fluids, 2024, 9(7): L072002.

Li, B., Yan, Z., Li, C., et al. Pore-scale experimental investigation on the co-current spontaneous imbibition of gaswater two-phase with gravity force. Physics of Fluids, 2023, 35: 117111.

Li, J., Fontelos, M. A. Drop dynamics on the beads-on-string structure for viscoelastic jets: A numerical study. Physics of Fluids, 2023,15(4): 922-937.

Mason, G., Morrow, N. R. Developments in spontaneous imbibition and possibilities for future work. Journal of Petroleum Science and Engineering, 2013, 110: 268-293.

Morozov, A., Van Saarloos, W. Subcritical instabilities in plane Poiseuille flow of an Oldroyd-B fluid. Journal of Statistical Physics, 2019, 175: 554-577.

Niedzwiedz, K., Wischnewski, A., Pyckhout-Hintzen, W., et al. Chain dynamics and viscoelastic properties of poly (ethylene oxide). Macromolecules, 2008, 41(13): 4866-4872.

Oldroyd, J. G. On the formulation of rheological equations of state. Proceedings of the Royal Society A, 1950, 200: 523-541.

Roychaudhuri, B., Tsotsis, T. T., Jessen, K., et al. An experimental investigation of spontaneous imbibition in gas shales. Journal of Petroleum Science and Engineering, 2013, 111: 87-97.

Shan, F., Chai, Z., Shi, B. A theoretical study on the capillary rise of non-Newtonian power-law fluids. Applied Mathematical Modelling, 2020, 81: 768-786.

Sheng, J. J. What type of surfactants should be used to enhance spontaneous imbibition in shale and tight reservoirs? Journal of Petroleum Science and Engineering, 2017, 159: 635-643.

Sonker, M., Bajpai, S., Khan, M. A., et al. Review of recent advances and their improvement in the effectiveness of hydrogel-based targeted drug delivery: A hope for treating cancer. ACS Applied Bio Materials, 2021, 4(12): 8080-8109.

Tani, M., Kawano, R., Kamiya, K., et al. Towards combinatorial mixing devices without any pumps by open-capillary channels: Fundamentals and applications. Scientific reports, 2015, 5(1): 10263.

Thompson, R. L., Oishi, C. M. Reynolds and Weissenberg numbers in viscoelastic flows. Journal of Non-Newtonian Fluid Mechanics, 2021, 292: 104550.

Vachaparambil, K. J., Einarsrud, K. E. Comparison of surface tension models for the volume of fluid method. Processes, 2019, 7: 542.

Wang, Y., Ye, D., Zhu, X., et al. Spontaneous imbibition in paper-based microfluidic devices: Experiments and numerical simulations. Langmuir, 2022, 38: 2677-2685.

Washburn, E. W. The dynamics of capillary flow. Physical Review, 1921, 17(3): 273-283.

Xia, Y., Xu, S., Cai, J., et al. Characterization and capillary pressure curve estimation of clayey-silt sediment in gas hydrate reservoirs of the South China Sea. Advances in Geo-Energy Research, 2023, 10(3): 200-207.

Xie, C., Balhoff, M. T. Lattice Boltzmann modeling of the apparent viscosity of thinning-elastic fluids in porous media. Transport in Porous Media, 2021, 137: 63-86.

Xie, C., Qi, P., Xu, K., et al. Oscillative trapping of a droplet in a converging channel induced by elastic instability. Physical Review Letters, 2022a, 128(5): 054502.

Xie, C., Xu, K., Qi, P., et al. A new mechanism of viscoelastic fluid for enhanced oil recovery: Viscoelastic oscillation. Advances in Geo-Energy Research, 2022b, 6(3): 267-268.

Yang, G. and Wang, M. Surface roughness effect on dynamic wettability in imbibition process. Computers & Fluids, 2023, 263: 105959.

Yang, S., Sheng, Q., Zou, M., et al. The influence of gravity on the fractal model of imbibition in rough pores considering shape factor. Chinese Journal of Physics, 2025, 96: 1261-1271.

Zhang, G., Ma, L., Tong, B., et al. Capillary rise behavior of lubricant in micropores with spiral bulge structures. Biomicrofluidics, 2023, 17: 024106.

Zheng, J., Lei, W., Ju, Y., et al. Investigation of spontaneous imbibition behavior in a 3D pore space under reservoir condition by lattice Boltzmann method. Journal of Geophysical Research: Solid Earth, 2021, 126(6): e2021JB021987.